

ORIGINAL RESEARCH

Open Access



Roles of nanoparticles and heat generation/absorption on MHD flow of Ag-H₂O nanofluid via porous stretching/shrinking convergent/divergent channel

Ashish Mishra¹, Alok Kumar Pandey^{2*}, Ali J. Chamkha³ and Manoj Kumar¹

* Correspondence: mrl.alokpandey1@gmail.com;
dralokpandey@yahoo.com

²Department of Mathematics,
Graphic Era Deemed to be
University, Dehradun, Uttarakhand
248002, India

Full list of author information is
available at the end of the article

Abstract

This article unveils the combined impact of heat generation/absorption and Joule heating on MHD flow of Ag-H₂O nanofluid into a porous stretching/shrinking divergent/convergent channel with viscous dissipation and solid volume fraction. The mathematical modeling is presented for the existing equations of continuity, momentum, and energy fraction. The reduced boundary value problem is solved numerically employing Runge-Kutta-Fehlberg (RKF) method via shooting scheme and then the outcomes are sketched and interpreted. The results explore that the thermal boundary layer thickness of the stretching divergent and the shrinking divergent channels enhance by increasing the value of the Eckert number, while the opposite tendency is scrutinized on the momentum boundary layer thickness by increasing the value of the porosity parameter for the stretching divergent and the shrinking convergent channels.

Keywords: Heat generation/absorption, Joule heating, Nanofluid, Porous media, Stretching/shrinking channel, Viscous dissipation

2010 Mathematics Subject Classifications: 80A20, 76S05, 76W05

Introduction

The study of fluid flow over convergent/divergent walls has extremely remarkable practical applications in the sector of science and engineering as well as in the domain of industrial and architectural works, for example, flows through cavity and canals. Another example of fluid flow via converging/diverging channels includes blood flow through arteries and capillaries in human body. Sheikholeslami et al. [1] illustrated the influence of nanoparticles and high Lorentz force on Jeffery-Hamel flow. The related non-linear equations are explained by Adomian decomposition technique and it was found that increase in Reynolds number led to reduction in the velocity near the walls. Convergent/divergent channels have certain practical applications such as industrial casting of metal, preparation of plastic sheets, molten metal streams control, manufacturing of fibers glasses, papers, and wires, in the presence of magnetic field. Turkyilmazoglu [2] analyzed the well-established Jeffery-Hamal fluid flow through shrinking/

stretching divergent/convergent channels. He found some exact solutions of governing nonlinear equations and proved that heat transfer rate enhanced near the channel walls due to increase in stretching parameter. The DRA is applied by Dogonchi and Ganji [3] to explore the impact of thermal radiation on magnetohydrodynamic nanofluid flow due to stretchable/shrinkable channels. They found that the fluid velocity increases with stretching parameter. The analytical outcomes of MHD copper-water nanofluid flow through two non-comparable converging/diverging channels with the help of RVI method was proposed by Azimi and Riazi [4]. They noted that increase in Eckert number resulted into increase in the values of Nusselt number. Khan et al. [5] examined the Soret-Dufour effects on MHD chemically reacting fluid flow via diverging and converging channels and the analytical solutions of existing flow equations were obtained by HAM (Homotopy Analysis Method). They revealed that when there was increase in Reynolds number, the opposite variations were observed in temperature profiles of convergent and divergent channels. Usman et al. [6] applied least square method to study the heat transportation attributes of two types of solid metal-water MHD nanofluid flow along a converging/diverging channel. Their study established that enhanced behavior of volume fraction of nanoparticles diminished the temperature fields. Impact of radiation on flow of Jeffry fluid towards stretchable diverging as well as converging channels was proposed by Ahmed et al. [7]. In their study, it was mentioned that increase in the values of Reynolds number reduced the velocity of shrinking divergent channel and consistently increased the shrinking convergent channel velocity. Several researchers have also studied convergent/divergent channels under different physical conditions [8–11].

The well-known physical quantity viscous dissipation is defined as a heat source which generates large amount of temperature in any medium. In permeable media, for example, stretching/shrinking surface, it is the rate at which kinetic energy is converted into heat per unit mass. Numerical investigation on convective flow of nanofluid using RKF technique over stretching/shrinking surface under the performance of viscous dissipation was conducted by Pal and Mandal [12]. They achieved the dual solution for velocity and temperature field for high values of existing parameters of shrinking sheet. Hayat et al. [13] demonstrated boundary layer problem of hydro-magnetic Williamson liquid past a permeable stretched sheet in the occurrence of Ohmic dissipation. From their study, they obtained that the surface drag force is augmented with magnetic field. A mixed convection electrical MHD flow of nanofluid and slip boundary condition on an elongate sheet was investigated by Hsiao [14], where they revealed that heat transfer rate increases as stagnation parameter values augmented. Kayalvizhi et al. [15] explored numerically the influences of slip condition on heat mass flux of MHD flow on incompressible fluid along a stretched surface with Ohmic dissipation in addition to viscous dissipation effect. They also showed that the surface drag force reduced due to magnetic field and increased with slip boundary conditions. Singh et al. [16] used analytical method to solve governing equations of micropolar fluid due permeable shrinking surface. In their investigation, they revealed that heat transfer accelerated due to Biot and Prandtl numbers at fluid solid interface. Pandey and Kumar [17] demonstrated the combined influence of radiation and heat generation/absorption on nanofluid flow through an unsteady stretching sheet. They also found that the rate of heat transfer declined as there was increase in the heat generation/absorption values. Similarly, in several other studies, the characteristic of heat transfer was analyzed due to the fluid flow

over stretching sheet [18–20]. Ganga et al. [21] explored viscous and Ohmic dissipation effects on MHD flow subjected to an upright plate in addition to heat generation/absorption effect on nanofluid. They explained that the temperature distribution declined due to increase in solid particles volume fraction. Singh et al. [22] studied the influence of MHD and slip velocity on flat plate due to alumina-water nanofluid and also discussed that the heat transfer rate moved faster as volume fraction of solid particle increased. Mishra et al. [23] discussed numerical method for existing equation of MHD Ag–H₂O nanofluid flow through a vertical cone with viscous-Ohmic dissipation and also described that the mass transfer rate declined as velocity slip parameters values increased. Chamkha et al. [24] utilized the finite difference method to solve the governing equations of boundary layer flow of vertical plate. Mishra et al. [25] explained the impacts of suction/injection and viscous dissipation on nanofluid flow via a stretching cylinder and revealed that temperature profiles reduced due to the increase in suction parameter values. Alamri et al. [26] deliberated the mass transfer impact on MHD flow of second grad fluid over stretching surface. They found that the velocity of fluid decelerated with increase in the magnetic parameter values. Ellahi et al. [27] studied the impacts of entropy generation and radiation on MHD nanofluid flow of through a wavy channel and revealed that the lower wall of channel energy was reduced due to radiation parameter. The studies related to the characteristics of heat transfer of various MHD nanofluids flow due to different geometry were performed by [28–30].

The aim of the present study is to fill the gaps that have been derived from the above mentioned published articles. The major objective is to figure out the physical aspects of MHD flow of Ag–water nanofluid in stretchable/shrinkable divergent/convergent channels subjected to the physical effects of heat generation/absorption, viscous dissipation, and Joule heating with involvement of porous media via the fourth–fifth order of the Runge-Kutta-Fehlberg scheme with the shooting algorithm.

Mathematical formulation

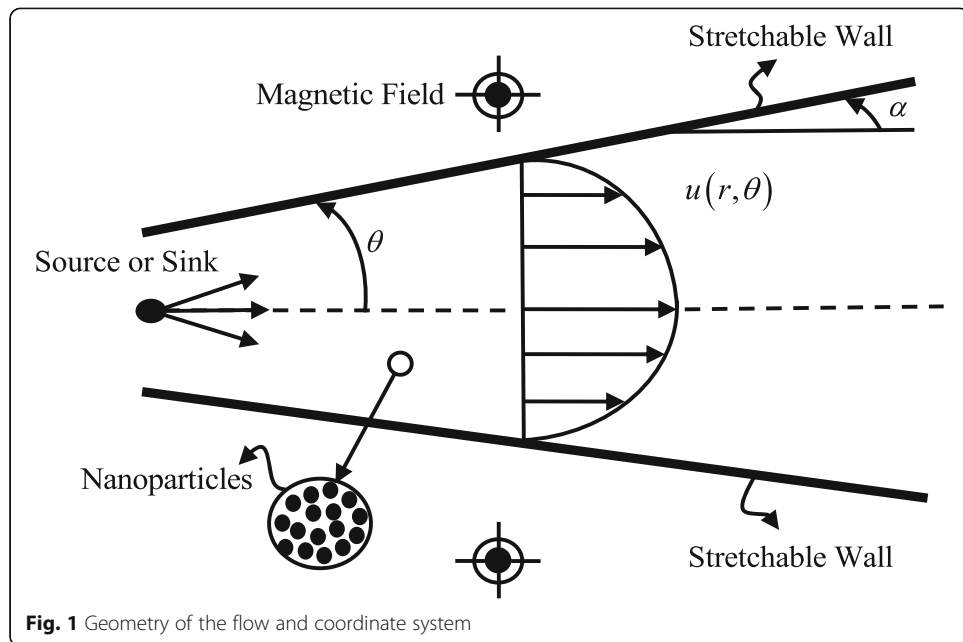
Considering a laminar, two-dimensional steady, and incompressible MHD flow of a nanofluid from a sink/source between two stretchable/shrinkable channels which make an angle 2α (Fig. 1).

Let the channels be assumed as radially shrinking/stretching according to $u = u_w = sr^{-1}$.

(1)

where the velocity is taken as $u = u(r, \theta)$ and the stretching/shrinking rate is s . Also, the surface temperature of the wall of channels is taken as T . The channels are assumed to be divergent, if $\alpha > 0$ and convergent, if $\alpha < 0$. It is taken for granted that the velocity is along the radial direction and subjected to both (r, θ) . In addition, the magnetic field is along the z -axis, and considering the efforts of Dogonchi and Ganji [3], the fundamental constitutive dimensional equations of the nanofluid, such as conservation of mass and energy equations in cylindrical coordinates can be written as [3, 11]:

Mass conservation equation



$$\frac{\rho_{nf}}{r} \frac{\partial}{\partial r} (ru) = 0 \quad (2)$$

Momentum equations

$$u \frac{\partial u}{\partial r} = - \frac{1}{\rho_{nf}} \left(\frac{\partial P}{\partial r} \right) - \frac{1}{\rho_{nf}} \left(\frac{\sigma_{nf} B_0^2}{r^2} + \frac{\mu_{nf}}{K} \right) u + \frac{\mu_{nf}}{\rho_{nf}} \left(\frac{\partial^2 u}{\partial r^2} + \frac{1}{r} \frac{\partial u}{\partial r} + \frac{1}{r^2} \frac{\partial^2 u}{\partial \theta^2} - \frac{u}{r^2} \right) \quad (3)$$

$$\frac{1}{\rho_{nf} r} \frac{\partial P}{\partial \theta} - \frac{2\mu_{nf}}{\rho_{nf} r^2} \frac{\partial u}{\partial \theta} = 0 \quad (4)$$

Energy equation

$$\begin{aligned} u \frac{\partial T}{\partial r} &= \frac{\kappa_{nf}}{(\rho C_p)_{nf}} \left(\frac{\partial^2 T}{\partial r^2} + r^{-1} \frac{\partial T}{\partial r} + r^{-2} \frac{\partial^2 T}{\partial \theta^2} \right) + \frac{\mu_{nf}}{(\rho C_p)_{nf}} \left[2 \left(\frac{\partial u}{\partial r} \right)^2 + 2r^{-2} u^2 + r^{-2} \left(\frac{\partial u}{\partial \theta} \right)^2 \right] \\ &+ \frac{1}{(\rho C_p)_{nf}} \left(\frac{Q_0}{r^2} T + \frac{\sigma_{nf}}{r^2} B_0^2 u^2 \right) - \frac{1}{(\rho C_p)_{nf} r} \left[\frac{\partial}{\partial r} (r q_{r,rad.}) + \frac{1}{r} \frac{\partial}{\partial \theta} (q_{\theta,rad.}) \right] \end{aligned} \quad (5)$$

In the above expressions, the fluid pressure is P and B_0 is the electromagnetic induction. Also, the physical aspects of silver nanoparticles and H_2O are shown in Table 1. The Hall effects and chemical reactions are neglected in the energy equation.

Table 1 Thermophysical characteristics of H_2O and Ag–nanoparticle (see [23])

	C_p	κ	ρ	σ
H_2O	997.1	4179	0.613	0.05
Ag	10500	235	429	6.3×10^7

The radiative heat flux $q_{r, rad}$ and $q_{\theta, rad}$ are supposed in r and θ directions, respectively. Now, as stated by Rosseland approximation [3, 11], $q_{r, rad}$ and $q_{\theta, rad}$ can be written as

$$q_{r,rad} = \frac{-16\sigma^* T_0^3}{3\kappa_{nf}^*} \frac{\partial T}{\partial r}, \quad q_{\theta,rad} = \frac{-16\sigma^* T_0^3}{3\kappa_{nf}^*} \frac{\partial T}{\partial \theta} \quad (6)$$

Here, κ_{nf}^* is the absorption coefficient and σ^* is the Stefan-Boltzmann constant, respectively. Now, substituting the values of Eq. (6) into Eq. (5), we get

$$\begin{aligned} u \frac{\partial T}{\partial r} &= \frac{\kappa_{nf}}{(\rho C_p)_{nf}} \left(\frac{\partial^2 T}{\partial r^2} + r^{-1} \frac{\partial T}{\partial r} + r^{-2} \frac{\partial^2 T}{\partial \theta^2} \right) - \frac{16\sigma^* T_\infty^3}{(\rho C_p)_{nf} 3\kappa_{nf}^*} \left(\frac{\partial^2 T}{\partial r^2} + r^{-1} \frac{\partial T}{\partial r} + \frac{\partial^2 T}{\partial \theta^2} \right) \\ &\quad + \frac{\mu_{nf}}{(\rho C_p)_{nf}} \left[2 \left(\frac{\partial u}{\partial r} \right)^2 + 2r^{-2} u^2 + r^{-2} \left(\frac{\partial u}{\partial \theta} \right)^2 \right] + \frac{1}{(\rho C_p)_{nf}} \left(\frac{Q_0}{r^2} T + \frac{\sigma_{nf}}{r^2} B_0^2 u^2 \right) \end{aligned} \quad (7)$$

The auxiliary conditions at boundary are

$$\left. \begin{aligned} u \frac{\partial T}{\partial r} &= \frac{\partial T}{\partial \theta} = 0, u = \frac{u_c}{r} \text{ at } \theta \rightarrow 0, \\ u = u_w &= \frac{s}{r}, \quad T = \frac{T_w}{r^2} \text{ as } \theta \rightarrow \pm \alpha \end{aligned} \right\} \quad (8)$$

Let us consider only radial flow, and then Eq. (1) is expressed as

$$f(\theta) = ru(r, \theta) \quad (9)$$

Thermo-physical properties of nanofluid

The physical terms effective density, heat capacitance, dynamic viscosity, thermal conductivity, and electric conductivity can be expressed as follows [11, 12]:

$$\left. \begin{aligned} \rho_{nf} &= \phi\rho_s + (1-\phi)\rho_f, \quad (\rho C_p)_{nf} = \phi(\rho C_p)_s + (1-\phi)(\rho C_p)_f, \\ \frac{\mu_{nf}}{\mu_f} &= (1-\phi)^{-2.5}, \quad \frac{\kappa_{nf}}{\kappa_f} = \frac{\kappa_s + 2\kappa_f - 2\phi(\kappa_f - \kappa_s)}{\kappa_s + 2\kappa_f + 2\phi(\kappa_f - \kappa_s)}, \\ \sigma_{nf} &= \phi\sigma_s + (1-\phi)\sigma_f \end{aligned} \right\} \quad (10)$$

where ϕ is volumetric fraction of Ag-nanoparticles, also subscripts s and f denote nano-silver particles and regular fluid, respectively.

Introduction of non-dimensional variables

We introduce the subsequent non-dimensional transformations to change the prevailing equations into set of ODEs [3, 11]:

$$f = \frac{f(\theta)}{u_c}, \quad \theta(\eta) = r^2 \frac{T}{T_w}, \quad \eta = \frac{\theta}{\alpha} \quad (11)$$

Incorporating Eqs. (10) and (11) into Eqs. (3) and (5), consequent system of non-linear ODEs can be yielded as

$$f''' + 2\alpha A_1 \operatorname{Re}(1-\phi)^{2.5} ff' + \left(4 - (1-\phi)^{2.5} Ha \right) \alpha^2 f' - K_1 f = 0 \quad (12)$$

$$(1 + Rd)\theta'' + 2\alpha^2 \left(\frac{A_2}{A_3} Prf + 2 + 2Rd + \frac{1}{2A_2} Q \right) \theta + \frac{1}{A_3(1-\phi)^{2.5}} \frac{EcPr}{Re} (4\alpha^2 f^2 + f'^2) \\ + \alpha \left(\frac{A_4 Ha Ec Pr}{A_3} \right) f^2 = 0 \quad (13)$$

The converted boundary condition in form of $f(\eta)$ and $\theta(\eta)$ are

$$\left. \begin{array}{l} f(\eta = 0) = 1, \quad f'(\eta = 0) = 0, \quad \theta'(\eta = 0) = 0, \\ f(\eta = 1) = \lambda, \quad \theta(\eta = 1) = 1 \end{array} \right\} \quad (14)$$

where prime indicates derivative w.r.t. η . The dimensionless existing parameters are characterized as follows: $\lambda (= \frac{s}{u_c}) < 0$ is shrinking parameter, $\lambda (= \frac{s}{u_c}) > 0$ is stretching parameter, $Rd (= \frac{16\sigma^* T_\infty^3}{3\kappa_{nf} K_f^*})$ is radiation parameter, $K_1 (= \frac{v_f}{K})$ is porosity parameter, $Ha (= \frac{\sigma_f B_0^2}{\rho_f v_f})$ is Hartmann number, $Pr (= \frac{u_c(\rho C_p)_f}{\kappa_f})$ is Prandtl number, $Re (= \frac{\alpha u_c}{v_f})$ is Reynolds number, $Q (= \frac{Q_0}{\kappa_f})$ is heat generation/absorption parameter, $Ec [= \frac{\alpha u_c^2}{T_w(C_p)_f}]$ is Eckert number, $A_1 [= \phi(\frac{\rho_s}{\rho_f}) + (1-\phi)]$, $A_2 [= \phi(\frac{\rho C_p)_s}{(\rho C_p)_f} + (1-\phi)]$, $A_3 \{ = \frac{2[\kappa_f - \phi(\kappa_f - \kappa_s)] + \kappa_s}{2[\kappa_f + \phi(\kappa_f - \kappa_s)] + \kappa_s} \}$, and $A_4 [= \phi(\frac{\sigma_s}{\sigma_f}) + (1-\phi)]$ are constants, respectively.

The significant values for engineering aspects such as skin friction coefficient and Nusselt number are

$$C_f^* = \left| \frac{\mu_{nf}}{\rho_f} f'(1) \right|, Nu^* = \left| \frac{\kappa_{nf}}{\kappa_f} \alpha^{-1} (1 + Rd) \theta'(1) \right| \quad (15)$$

Numerical method

The two-dimensional flow of the nanofluid by incorporating silver as nanoparticles is formulated. The highly non-linear momentum (12) and energy (13) equations associated with the auxiliary boundary condition (14) are solved numerically by taking the RKF45 technique in conjunction with the shooting procedure. One of the main advantages of the shooting process is that it contains a fifth-order truncation error and the procedure of computation of solutions is very easy as compared to other numerical methods, so the purpose of this technique is to deal with IVP (initial value problem), thus non-dimensional leading equations, such as Eq. (12) and Eq. (13) are converted to first order. Thus, these equations can be re-arranged as follows:

$$f''' = -2\alpha A_1 Re(1-\phi)^{2.5} ff' - \left(4 - (1-\phi)^{2.5} Ha \right) \alpha^2 f' + K_1 f \quad (16)$$

$$\theta'' = \frac{1}{(1 + Rd)} \begin{bmatrix} -2\alpha^2 \left(\frac{A_2}{A_3} Prf + 2 + 2Rd + \frac{1}{2A_2} Q \right) \theta \\ -\frac{(1-\phi)^{-2.5}}{A_3} \frac{EcPr}{Re} (4\alpha^2 f^2 + f'^2) \\ -\alpha \left(\frac{A_4 Ha Ec Pr}{A_3} \right) f^2 \end{bmatrix} \quad (17)$$

Further step is to alter Eq. (18) into a set of first-order ODEs by defining other variables such as

$$\left. \begin{array}{l} f = y_1, f' = y_2, f'' = y_3, \\ \theta = y_4, \theta' = y_5. \end{array} \right\} \quad (18)$$

After imposing Eq. (18) into Eqs. (16) and (17), we obtained subsequent arrangement of first-order equations:

$$\left. \begin{array}{l} y'_1 = y_2 \\ y'_2 = y_3 \\ y'_3 = -2\alpha Re A_1 (1-\phi)^{2.5} y_1 y_2 \\ \quad - \left(4 - (1-\phi)^{2.5} Ha A_4 \right) \alpha^2 y_2 + K_1 y_1 \\ y'_4 = y_5 \\ \quad - 2\alpha^2 \left(\frac{A_2}{A_3} P r y_1 + 2 \right. \\ \quad \left. + 2 R d + \frac{Q}{2 A_3} \right) y_4 - \alpha A_4 \left(\frac{Ha E c P r}{A_3} \right) y_1 y_1 \\ y'_5 = \frac{-\frac{(1-\phi)^{-2.5} E c P r}{A_3 R e} (4\alpha^2 y_1 y_1 + y_2 y_2)}{(1 + R d)} \end{array} \right\} \quad (19)$$

Subsequently, the corresponding boundary conditions are

$$\left. \begin{array}{l} y_1(0) = 1, y_2(0) = 0, y_3(0) = t_1, \\ y_4(0) = t_2, y_5(0) = 0, \\ y_2(1) = \lambda, y_4(1) = 1. \end{array} \right\} \quad (20)$$

Since the above created set have five first-order equations, thus the solution of the system can be achieved, if five initial conditions are known. In Eq. (20), there are only five conditions are identified. The Eq. (19) along with Eq. (20) as IVP, here we require the values of missing slopes $t_1 = f'(0)$ and $t_2 = \theta'(0)$. As values of t_1 and t_2 are unknown, we begin with given initial values of $f' = \lambda$ and $\theta = 1$ for a suitable fixed length η_∞ . The step size is taken $\Delta\eta = 10^{-3}$. The boundary conditions in Eq. (20) are estimated utilizing $\eta_{\max} = 1$ as

$$f'(\eta_{\max=1}) \rightarrow \lambda \text{ and } \theta(\eta_{\max=1}) \rightarrow 1 \quad (21)$$

The convergence criterion is chosen less than 10^{-10} to obtain the numerical solution. If calculated outcome does not meet convergence criteria, in that case, initial approximated values are modified via Newton's technique. The aforesaid process is done again and again until an iteration limit is attained or desired accuracy is accomplished.

Code validation

We have compared skin factor $f'(1)$ and Nusselt number $-\theta'(1)$ for diverse values of λ at different values with the already studied by Turkyilmazoglu [2] and Dogonchi and Ganji [3] to justify our numerical procedure under limiting sense. An excellent agreement has been obtained on observing Table 2, which justifies the reliability of our present numerical data.

Table 2 Comparison of numerical value of $f'(1)$, for various values of stretching/shrinking parameter λ and divergent/convergent parameter α , when $Re = 50$ and $\varphi = 0$

λ	α	Turkyilmazoglu [2]		Dogonchi and Ganji [3]		Present result	
		$f'(1)$	$-\theta'(1)$	$f'(1)$	$-\theta'(1)$	$f'(1)$	$-\theta'(1)$
-2	-5	-5.130921689	0.03157845854	-5.1309222926	0.0315761821	-5.1309318671	0.0315752477
-1	-5	-4.652183982	0.03734696604	-4.6521591354	0.0373226368	-4.6521592892	0.0373210205
0	-5	-2.833915413	0.04214811723	-2.8339514330	0.0421517243	-2.8338418752	0.0421520009
2	-5	3.654305033	0.05052578617	3.6697111853	0.0502423154	3.5697079349	0.0502430863
-1	5	-3.508090102	0.03475109986	-3.5081031667	0.0347758169	-3.5080681268	0.0347755158
0	5	-1.109360533	0.03999321083	-1.1093265266	0.0399820121	-1.1092617837	0.0399841412
1	5	0	0.04640127099	0	0.0464015106	0	0.0464037895

Results and discussion

The converted radial hydro-thermal equations, i.e., (12) and (13) with respect to boundary conditions (14) are numerically illuminated utilizing RKF45 procedure with shooting algorithm. The influences of assorted physical aspects, such as Hartmann number (Ha), heat generative/absorptive parameter (Q), porosity parameter (K_1), Eckert number (Ec), and solid volumetric fraction (ϕ) of working nanoparticles are inspected on the profiles of velocity and temperature. Throughout this investigation for mathematical computations, the default values are set as $Re = 50$, $Pr = 6.2$, and $Rd = 0.2$. The physical parameters such as Hartmann number (Ha) lies in the domain of $[0, 4]$ and heat generation/absorption parameter $Q \in [-2, 1]$. Moreover, the values of other relevant parameters such as porosity parameter (K_1) and Eckert number (Ec) are varied as $0 \leq K_1 \leq 0.5$ and $0 \leq Ec \leq 0.05$, respectively. Any change from the default value is mentioned in the suitable figures and tables. Moreover, in all of the graphical explanations, a solid line represents the profile for divergent channel, while dashed line denotes the same for convergent channel.

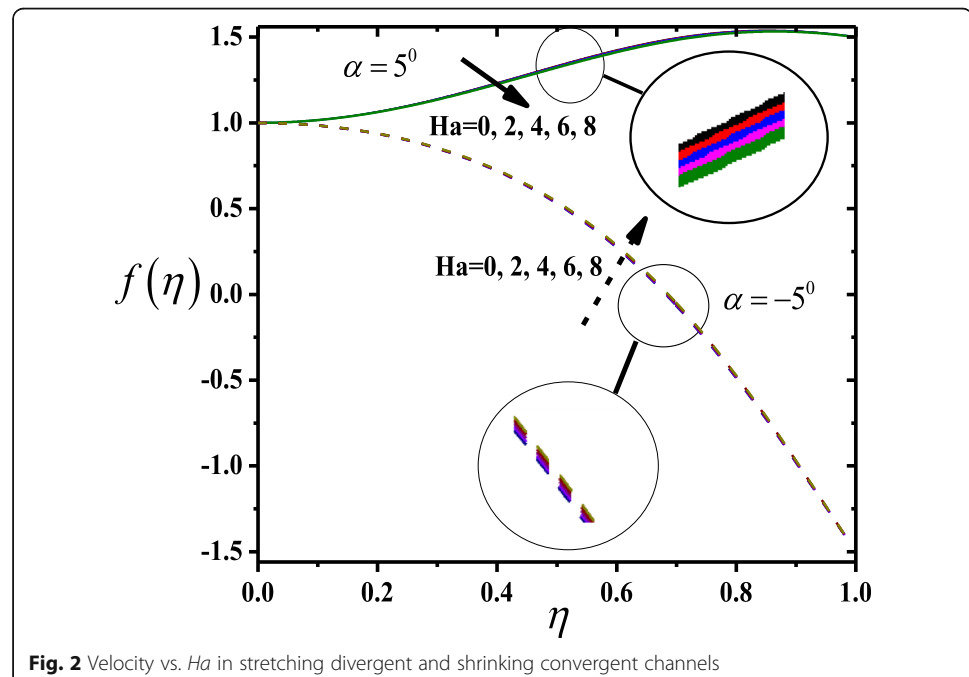
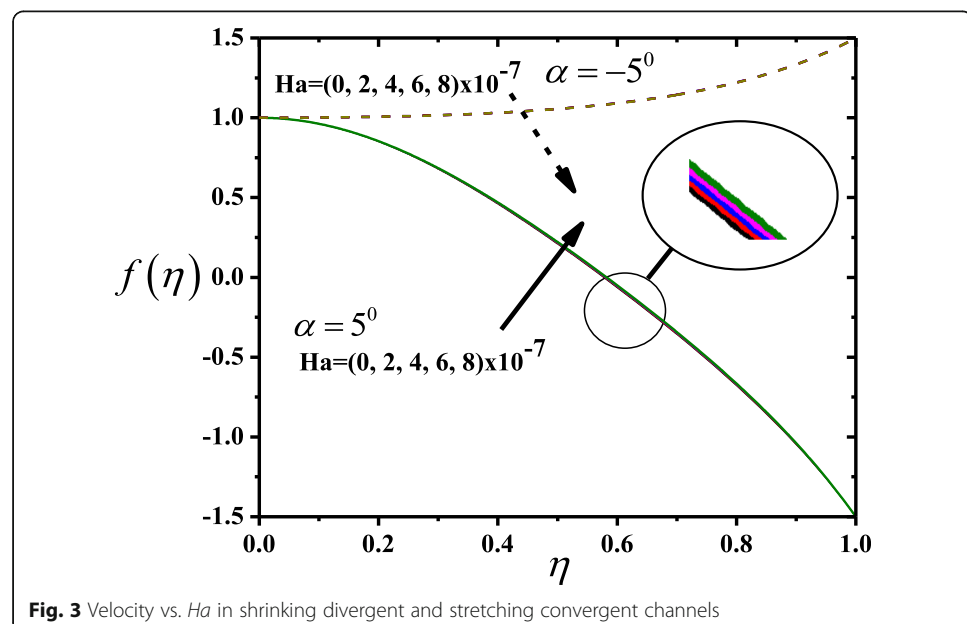


Fig. 2 Velocity vs. Ha in stretching divergent and shrinking convergent channels

Table 3 Several values of $f'(1)$ and $-\theta'(1)$ for stretching/divergent channel when $Re = 50$, $Pr = 6.2$, $\alpha = 5^0$, $Rd = 0.2$, and $\lambda = 1.5$

$Ha \times 10^{-7}$	K_1	Ec	Q	φ	$f'(1)$	$-\theta'(1)$
0	0.5	0.01	-2	5	-0.5317634576	1.0499021787
2					-0.5153347844	1.0849123020
4					-0.4998341256	1.1196884312
	0				-0.6677784568	1.1478237344
	0.2				-0.5964922157	1.1464838830
	0.4				-0.5265749221	1.1452279965
	0				-0.4919174596	1.0565571612
	0.01				-0.4919174596	1.1445716475
	0.05				-0.4919174596	1.4969913826
	-1				-0.4919174596	1.1400804534
	0				-0.4919174596	1.1431134675
	1				-0.4919174596	1.1461722611
	1				-0.1044674334	1.0828977870
	5				-0.4919000342	1.1445716464
	10				-0.9469547712	1.2054163788

The setting of stretching of divergent channel and shrinking of convergent channel on velocity profile is summarized for Hartmann number (Ha) in Fig. 2. It is noticeable from figure that an augmentation in Hartmann number decreases the velocity profile for stretching of divergent channel. This is due to small changes in the values of Hartmann number which corresponds to change in Lorentz force (by considering magnetic field effect). Consequently, the modified Lorentz force is responsible for an elevated resistance to the transfer of flow in case of stretching channel. Moreover, influence of Hartmann number in stretching/divergent channel is to produce more wall shear stress as mentioned in Table 3. When the shrinking/convergent channel is considered, the opposite nature has



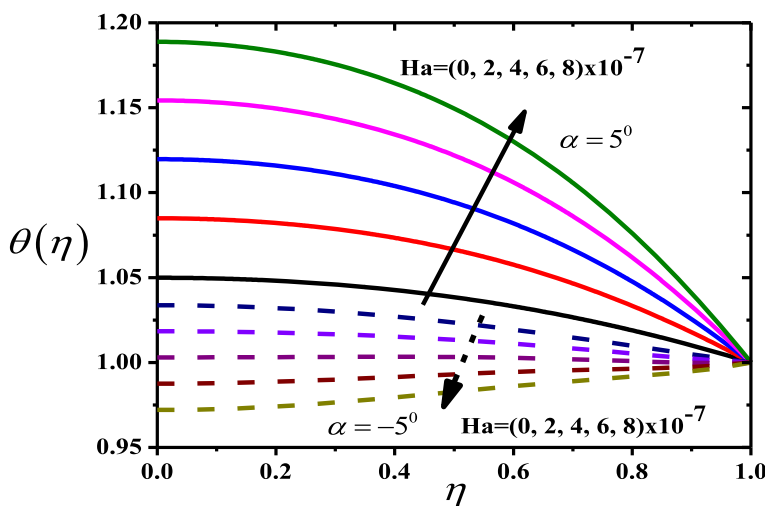


Fig. 4 Temperature vs. Ha in stretching divergent and shrinking convergent channels

been found so, by increasing Ha , the flow reversal disappears. Thus, velocity profile increases. Fig. 3 demonstrates that the effects of Hartmann number on velocity profile and wall shearing of the shrinking divergent channel are similar to those of the shrinking convergent channel. Also, a deceleration is observed on velocity field in stretching/convergent channel. Moreover, if there is a backflow in the shrinking channel, then Hartmann number can be used to lessen the backflows. Its inclusion also prevents the separation phenomena, resulting in a smooth flow.

The variation of temperature profile under the action of Hartmann number is illustrated in Fig. 4. It is witnessed that maximum amount of Hartmann number for stretching divergent channel corresponds to an increase in $\theta(\eta)$. Therefore, an excessive heating process occurs leading to increase of heat transfer rate and corresponding thermal layer, which is highlighted in Table 3. A temperature drop is examined in case of shrinking convergent channel. In other words, shrinking cools down the system by

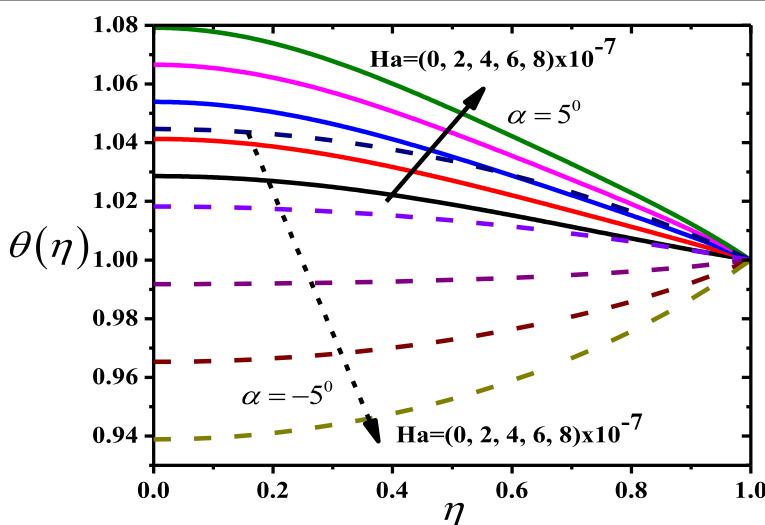
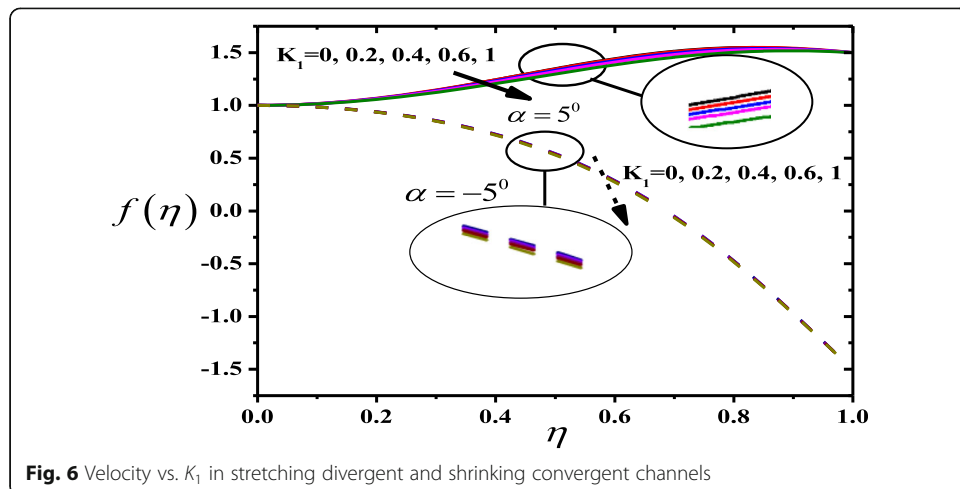
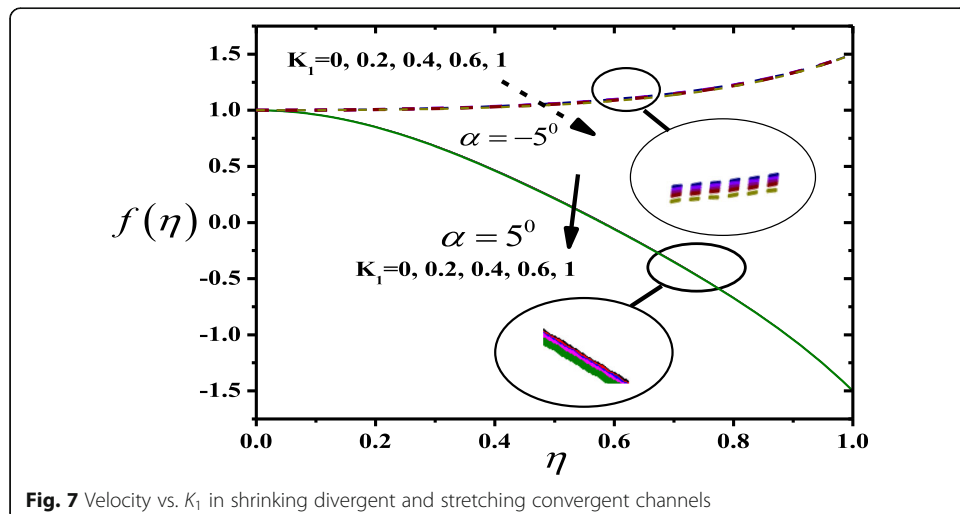


Fig. 5 Temperature vs. Ha in shrinking divergent and stretching convergent channels



reducing the thickness of thermal layer. Description of thermal field through shrinking/divergent and stretching/convergent channels for the various values of Ha is done with the help of Fig. 5. When the shrinking divergent channel is considered, the graph shows that the influence of Hartmann number on the thermal field is akin to those of stretching/divergent channel, whereas, opposite trend is observed in stretching/convergent channel.

The next set of figures (Figs. 6, 7, 8 and 9) explains the changes occurring in velocity and temperature profiles under the actions of porosity parameter (K_1) for stretching/shrinking convergent/divergent channel. Figure 6 shows distribution of velocity profile against η for assorted values of porosity parameter in case of stretching of divergent and shrinking of convergent channels. Velocity field is seen to decrease for higher values of porosity parameter in both channels. Physical explanation of this result lies in that fact that an increase in the value of porosity parameter directly related to decrease in permeability of the working medium. Thus, the medium with very less permeability is main reason for deceleration in fluid velocity. It becomes difficult to move for nano-fluid, so velocity decreases. The influence of porosity parameter on velocity profile in shrinking divergent and stretching convergent channels is captured in Fig. 7. The



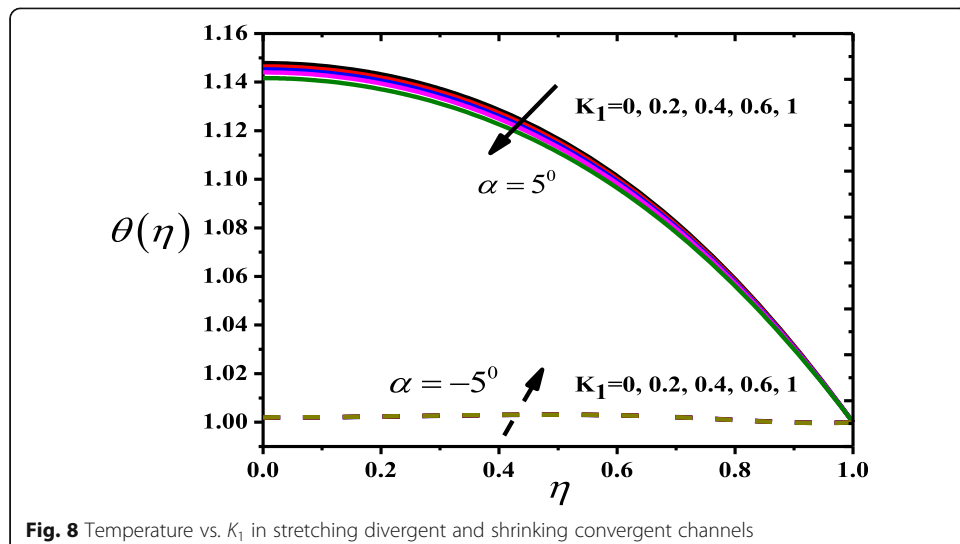


Fig. 8 Temperature vs. K_1 in stretching divergent and shrinking convergent channels

velocity profile displays same trend as above, i.e., larger porosity parameter creates a reduction in velocity distribution. Moreover, the absolute value of surface drag is decreased as porosity parameter increases. So, it results in release of very less amount of heat leads to temperature drop in stretching divergent channel (see Fig. 8). Also, an increase in porosity parameter causes less heat to be generated, thus a slight increment is observed in temperature distribution for shrinking convergent channel on enhancing K_1 in Fig. 8. We observed same scenario in Fig. 9 as for the influence on both the divergent and convergent channel in Fig. 8, i.e., porosity parameter reduces the temperature in shrinking divergent channel, while it shows reverse trend in stretching convergent channel.

Figures 10 and 11 are plotted to investigate the variation in thermal profiles due to the changes in Eckert number (Ec). Physically, Eckert number denotes the effect of viscous dissipation on thermal fields. As expected, Fig. 10 confirms that temperature in the vicinity of stretching divergent channel increases for large estimation of Ec , while a reduction can be observed in shrinking convergent channel. Generally, when the Eckert

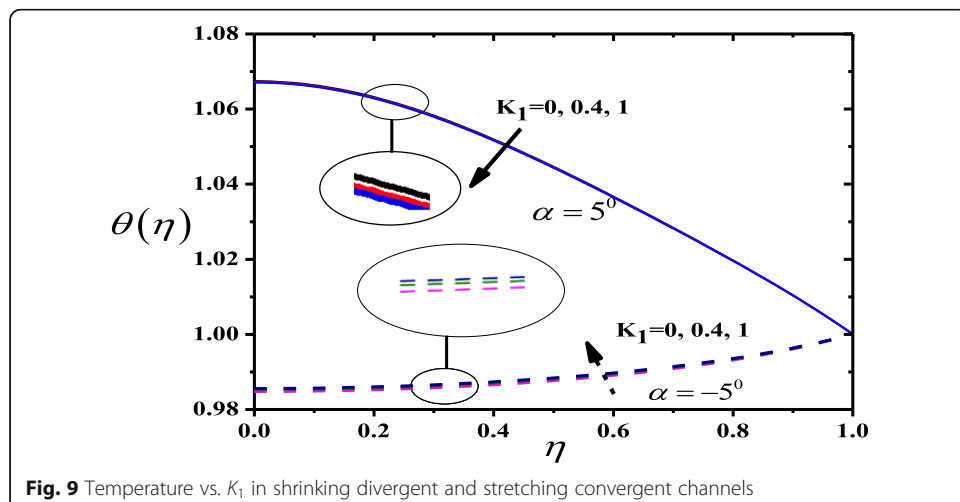
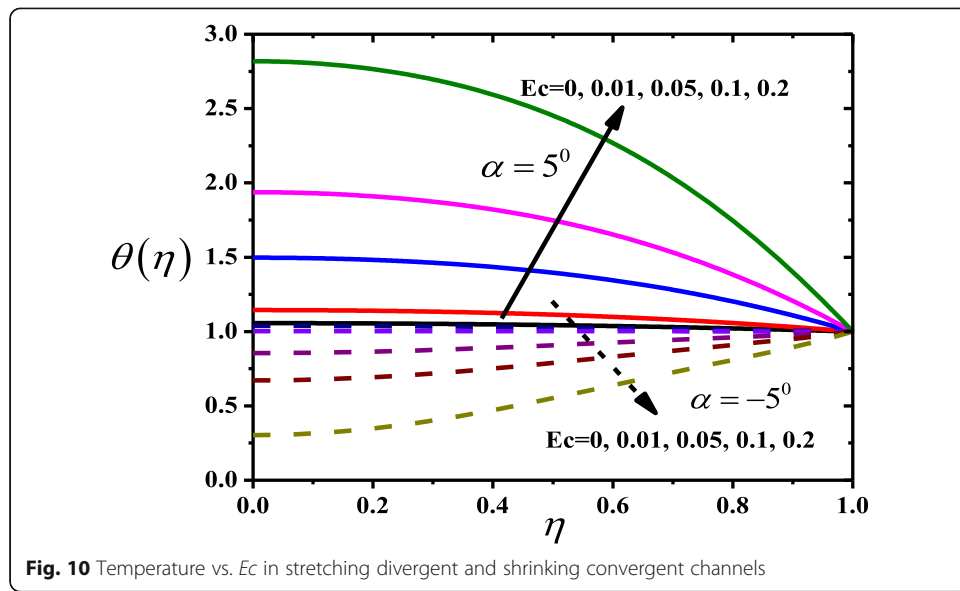
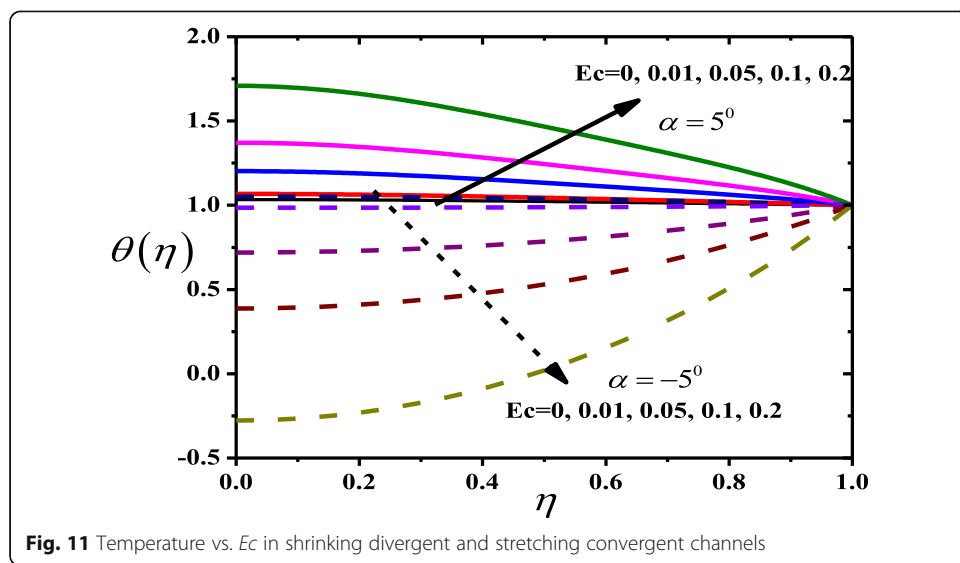


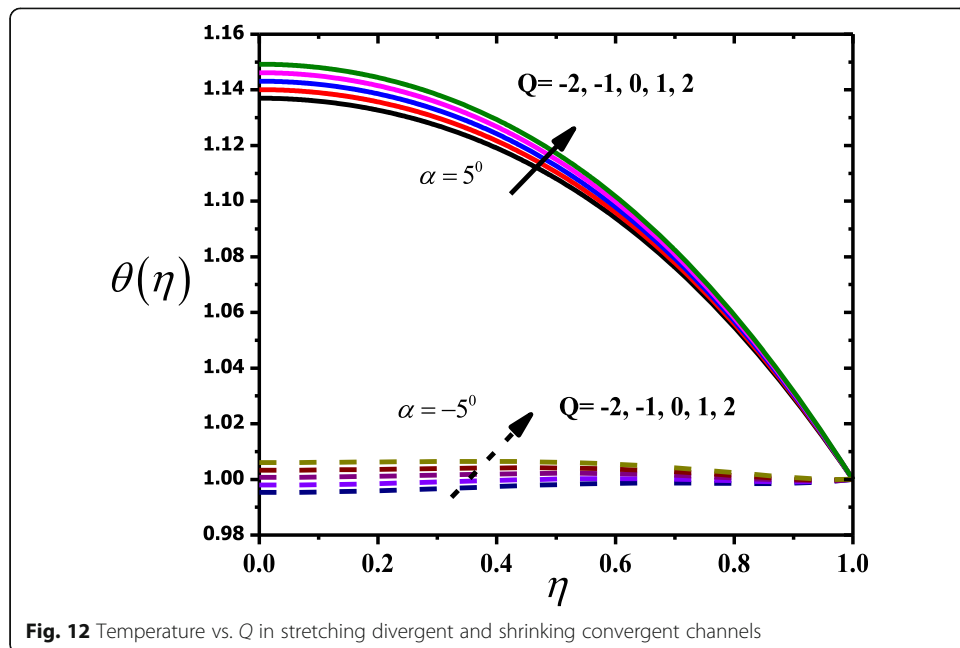
Fig. 9 Temperature vs. K_1 in shrinking divergent and stretching convergent channels



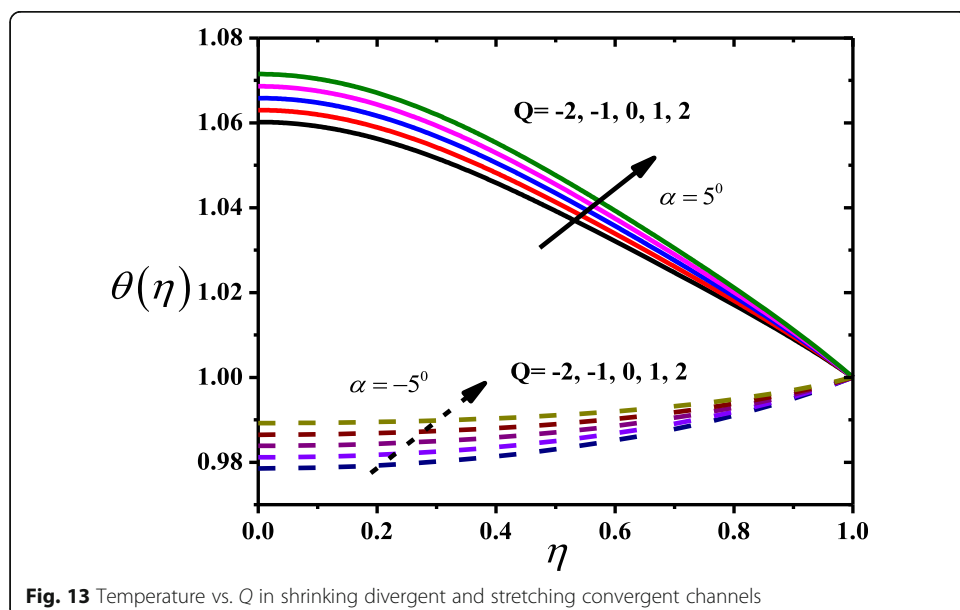
number increases, the fluid friction plays dominant role to increase the amount of heat thus, in stretched divergent condition, more fluid particles closer to wall and more friction creates significant amount of heat during this process. While a decrease is observed on temperature profile in case of shrinking convergent channel due to increase in Ec . Figure 11 is sketched to explore the differences in temperature profile subjected to shrinking divergent and stretching convergent channels under the impact of varying Eckert number. For shrinking divergent wall, it is interesting to see that thermal boundary layer escalates; normally dissipation under the influence of magnetic parameter creates heat in system known as Joule heating. On the other hand, temperature depreciates for stretching convergent channel under same setting.

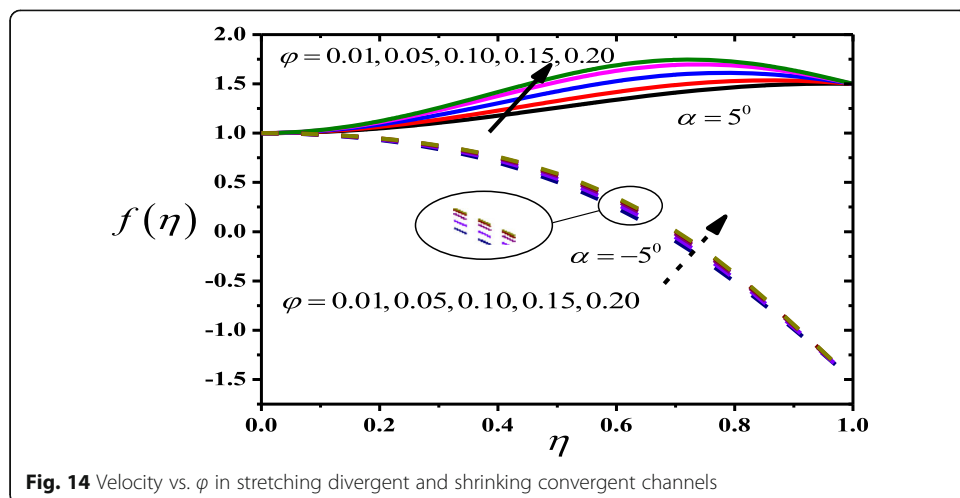
Figures 12 and 13 exhibit the response of heat generation/absorption parameter (Q) for stretching/shrinking channels under diverging/converging conditions. Here, physical parameters have fixed value such as $Pr = 6.2$, $\alpha = \pm 5^\circ$, $Ec = 0.01$, $\lambda = \pm 1.5$, $Rd = 0.2$,





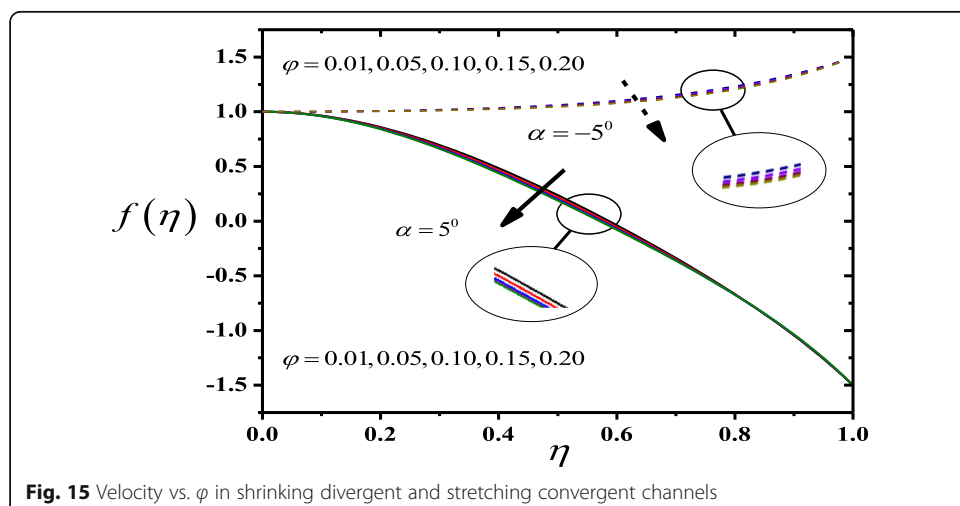
$\text{Re} = 50$, and $\text{Ha}=5\times 10^{-7}$. From the Fig. 12, it is concluded that thermal field of Ag–water nanofluid grows with increasing values of Q . Moreover; the associated boundary layer becomes wider with Q . Physically, dominating values of heat generation/absorption parameter leads additional heat to working fluid which is responsible for acceleration in thermal profile. Furthermore, it is evident from the Table 3 that the heat transfer rate is raised, when Q is augmented. Hence, it results in release of maximum amount of heat leads to hike in temperature in shrinking/divergent and stretching convergent channels (see Fig. 13). Thus, these results help us to figure out that, where the heating is desired, technically both the shrinking/stretching channels are favorable.

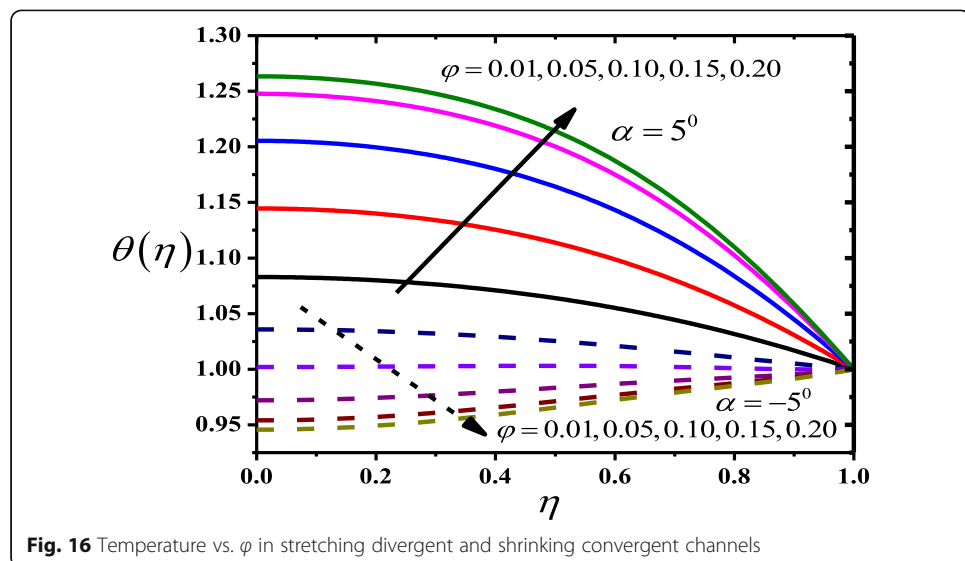




The description of velocity and thermal profiles through the various values of volume fraction parameter (ϕ) of Ag–nanoparticles in stretching/shrinking divergent/convergent wall is illustrated in Figs. 14, 15, 16, and 17. It is inspected for the conventional fluid ($\phi = 0$) that the numerical estimations of all constants become unity, i.e., $A_i = 1, \forall i \in [1, 4]$. From Fig. 14, a raise in ϕ enhances the velocity in both channels. Moreover, Table 3 shows that drag force is decelerated as ϕ increases. On the other hand, it is clear from Fig. 15 that, when H₂O-based nanofluid contains Ag–nanoparticles in its arrangement, then velocity profile decreases in both cases of shrinking divergent and stretching convergent channels. Physically, increasing volumetric fraction is directly related to higher concentration of nanoparticles in pure fluid. Thus, fluid become denser creates difficulty to flow through the medium, which leads to decrease in velocity.

Figure 16 demonstrates the features of volume fraction parameter on thermal distribution in stretching divergent and shrinking convergent channels. The graph shows that the temperature increases on adding the nanoparticles into the conventional fluid on stretching divergent channel. It is observable that there is a hike in the thermal conductivity on accelerating the amount of ϕ . Thus, the width of thermal boundary layer



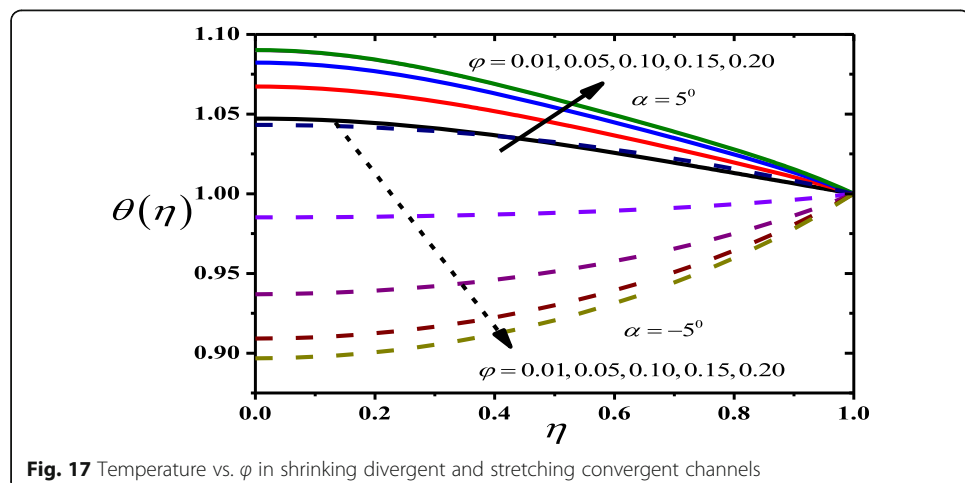


enhances extensively. Also, Table 3 confirms that heat transfer rate considerably enhanced as estimation of volumetric parameter increases. However, the shrinking convergent channel shows contrary behavior for same condition. In other words, the thermal boundary layer decreases on enhancing the value of φ in shrinking/convergent channel.

We finally discuss the performance of volume fraction parameter due to shrinking divergent and shrinking divergent in Fig. 17. The outline of the graph depicts that higher value of φ helps temperature to increase rapidly in shrinking divergent channel, while the reverse behavior can be seen in stretching convergent channel.

Conclusions

The present article investigated the flow analysis of MHD Ag–water nanofluid over stretching/shrinking divergent/convergent channel in porous medium. The effects of Hartmann number, porosity parameter, Eckert number, and nanoparticles volume fraction were incorporated. The major findings of current study are as follows:



- Opposite variations in velocity profile are investigated for varying Hartmann number in stretching divergent and shrinking convergent channels.
- Higher values of heat generation/absorption parameter led to increase in velocity and thermal profiles in shrinking convergent channels.
- Identical behavior of varying porosity parameter was observed in velocity profiles for both shrinking and stretching channels.
- The role of Hartmann number and dissipation parameter is to enhance the temperature of divergent channel but reverse effect is obtained for convergent channel.
- Heat transfer rate occur at a faster rate as the intensity of Hartmann number, nanoparticles volume fraction, Eckert number, and heat generation/absorption parameter are increased
- Higher values of porosity parameter led to increase in temperature field for convergent channel.
- The flow of nanofluid along the stretching convergent and shrinking divergent channels is reduced by silver nanoparticles volume fraction.

Acknowledgements

The authors wish to convey their sincere thanks to the reviewers for their valuable suggestions and comments for improving the manuscript quality.

Authors' contributions

A Mishra carried out the problem design and computation. AK Pandey was involved in the computation, code validation, draft preparation. AC Chamkha had a role in methodology and writing. M Kumar was involved in writing—original draft preparation. The authors read and approved the final manuscript.

Funding

The authors declare that they have no funding.

Availability of data and materials

All the data generated and materials during this study are included in this research article.

Competing interests

The authors declare that they have no competing interests.

Author details

¹Department of Mathematics, Statistics and Computer Science, G. B. Pant University of Agriculture and Technology, Pantnagar, Uttarakhand 263145, India. ²Department of Mathematics, Graphic Era Deemed to be University, Dehradun, Uttarakhand 248002, India. ³Mechanical Engineering Department, Prince Mohammad Bin Fahd University, Al-Khobar 31952, Saudi Arabia.

Received: 14 January 2020 Accepted: 13 April 2020

Published online: 22 April 2020

References

- Sheikholeslami, M., Ganji, D.D., Ashorynejad, H.R., Rokni, H.B.: Analytical investigation of Jeffery-Hamel flow with high magnetic field and nanoparticle by Adomian decomposition method. *Appl. Math. Mech.* **33**(1), 25–36 (2012) <https://doi.org/10.1007/s10483-012-1531-7>
- Turkyilmazoglu, M.: Extending the traditional Jeffery-Hamel flow to stretchable convergent/divergent channels. *Comput. Fluids.* **100**, 196–203 (2014) <https://doi.org/10.1016/j.compfluid.2014.05.016>
- Dogonchi, A.S., Ganji, D.D.: Investigation of MHD nanofluid flow and heat transfer in a stretching/shrinking convergent/divergent channel considering thermal radiation. *J. Mol. Liq.* **220**, 592–603 (2016) <https://doi.org/10.1016/j.molliq.2016.05.022>
- Azimi, M., Riazi, R.: MHD copper-water nanofluid flow and heat transfer through convergent-divergent channel. *J. Mech. Sci. Technol.* **30**(10), 4679–4686 (2016) <https://doi.org/10.1007/s12206-016-0938-3>
- Khan, U., Ahmed, N., Mohyud-Din, S.T.: Thermo-diffusion, diffusion-thermo and chemical reaction effects on MHD flow of viscous fluid in divergent and convergent channels. *Chem. Eng. Sci.* **141**, 17–27 (2016) <https://doi.org/10.1016/j.ces.2015.10.032>
- Usman, M., Haq, R.U., Hamid, M., Wang, W.: Least square study of heat transfer of water based Cu and Ag nanoparticles along a converging/diverging channel. *J. Mol. Liq.* **249**, 856–867 (2018) <https://doi.org/10.1016/j.molliq.2017.11.047>
- Ahmed, N., Abbasi, A., Khan, U., Mohyud-Din, S.T.: Thermal radiation effects on flow of Jeffery fluid in converging and diverging stretchable channels. *Neural Comput. Applic.* **30**(8), 2371–2379 (2018) <https://doi.org/10.1007/s00521-016-2831-5>

8. Asadullah, M., Khan, U., Ahmed, N., Mohyud-Din, S.T.: Analytical and numerical investigation of thermal radiation effects on flow of viscous incompressible fluid with stretchable convergent/divergent channels. *J. Mol. Liq.* **224**, 768–775 (2016) <https://doi.org/10.1016/j.molliq.2016.10.073>
9. Mohyud-Din, S.T., Khan, U., Ahmed, N., Bin-Mohsin, B.: Heat and mass transfer analysis for MHD flow of nanofluid in convergent/divergent channels with stretchable walls using Buongiorno's model. *Neural Comput. Appl.* **28**(12), 4079–4092 (2017) <https://doi.org/10.1007/s00521-016-2289-5>
10. Gerdroodbari, M.B., Takami, M.R., Ganji, D.D.: Investigation of thermal radiation on traditional Jeffery–Hamel flow to stretchable convergent/divergent channels. *Case Stud. Therm. Eng.* **6**, 28–39 (2015) <https://doi.org/10.1016/j.csite.2015.04.002>
11. Pandey, A.K., Kumar, M.: MHD flow inside a stretching/shrinking convergent/divergent channel with heat generation/absorption and viscous-Ohmic dissipation utilizing Cu-water nanofluid. *Comput Therm Sci: An Int J.* **10**(05), 457–471 (2018) <https://doi.org/10.1615/ComputThermalSci.2018020807>
12. Pal, D., Mandal, G.: Hydromagnetic convective-radiative boundary layer flow of nanofluids induced by a non-linear vertical stretching/shrinking sheet with viscous-Ohmic dissipation. *Powder Technol.* **279**, 61–74 (2015) <https://doi.org/10.1016/j.powtec.2015.03.043>
13. Hayat, T., Shafiq, A., Alsaedi, A.: Hydromagnetic boundary layer flow of Williamson fluid in the presence of thermal radiation and Ohmic dissipation. *Alexandria Eng. J.* **55**(3), 2229–2240 (2016) <https://doi.org/10.1016/j.aej.2016.06.004>
14. Hsiao, K.L.: Stagnation electrical MHD nanofluid mixed convection with slip boundary on a stretching sheet. *Appl. Therm. Eng.* **98**, 850–861 (2016) <https://doi.org/10.1016/j.applthermaleng.2015.12.138>
15. Kayalvizhi, M., Kalaiyanan, R., Ganesh, N.V., Ganga, B., Hakeem, A.A.: Velocity slip effects on heat and mass fluxes of MHD viscous-Ohmic dissipative flow over a stretching sheet with thermal radiation. *Ain Shams Eng. J.* **7**(2), 791–797 (2016) <https://doi.org/10.1016/j.asenj.2015.05.010>
16. Singh, K., Pandey, A.K., Kumar, M.: Analytical approach to a stagnation point flow and heat transfer of a micropolar fluid via a permeable shrinking sheet with slip and convective boundary conditions. *Heat Transf. Res.* **50**(8), 739–756 (2018) <https://doi.org/10.1615/HeatTransRes.2018024647>
17. Pandey, A.K., Kumar, M.: Effects of viscous dissipation and heat generation/absorption on nanofluid flow over an unsteady stretching surface with thermal radiation and thermophoresis. *Nanosc Technol: An Int J.* **9**(4), 325–341 (2018) <https://doi.org/10.1615/NanoSciTechnollntJ.2018025978>
18. Megahed, A.M.: Williamson fluid flow due to a nonlinearly stretching sheet with viscous dissipation and thermal radiation. *J Egyptian Math Soc.* **27**(1), 12 (2019) <https://doi.org/10.1186/s42787-019-0016-y>
19. Ibrahim, W., Negera, M.: MHD slip flow of upper-convected Maxwell nanofluid over a stretching sheet with chemical reaction. *J Egyptian Math Soc.* **28**(1), 7 (2020). <https://doi.org/10.1186/s42787-019-0057-2>
20. Elgazery, N.S.: Nanofluids flow over a permeable unsteady stretching surface with non-uniform heat source/sink in the presence of inclined magnetic field. *J Egyptian Math Soc.* **27**(1), 9 (2019) <https://doi.org/10.1186/s42787-019-0002-4>
21. Ganga, B., Ansari, S.M.Y., Ganesh, N.V., Hakeem, A.A.: MHD radiative boundary layer flow of nanofluid past a vertical plate with internal heat generation/absorption, viscous and Ohmic dissipation effects. *J. Nigerian Math. Soc.* **34**(2), 181–194 (2015) <https://doi.org/10.1016/j.jnms.2015.04.001>
22. Singh, P., Pandey, A.K., Kumar, M.: Forced convection in MHD slip flow of alumina-water nanofluid over a flat plate. *J Enhan Heat Transf.* **23**(6), 487–497 (2016) <https://doi.org/10.1615/JEnhHeatTransf.2018025485>
23. Mishra, A., Pandey, A.K., Kumar, M.: Velocity, thermal and concentration slip effects on MHD silver-water nanofluid past a permeable cone with suction/injection and viscous-Ohmic dissipation. *Heat Transf. Res.* **50**(14), 1351–1367 (2019). <https://doi.org/https://doi.org/10.1615/HeatTransRes.2018020420>
24. Chamkha, A.J., Al-Mudhaf, A., Pop, I.: Effect of heat generation or absorption on thermophoretic free convection boundary layer from a vertical flat plate embedded in a porous medium. *Int. Commun. Heat Mass Transf.* **33**, 1096–1102 (2006) <https://doi.org/10.1016/j.icheatmasstransfer.2006.04.009>
25. Mishra, A., Pandey, A.K., Kumar, M.: Ohmic-viscous dissipation and slip effects on nanofluid flow over a stretching cylinder with suction/injection. *Nanosc Technol: An Int J.* **9**(2), 99–115 (2018) <https://doi.org/10.1615/NanoSciTechnollntJ.2018025410>
26. Alamri, S.Z., Khan, A.A., Azeez, M., Ellahi, R.: Effects of mass transfer on MHD second grade fluid towards stretching cylinder: a novel perspective of Cattaneo–Christov heat flux model. *Phys. Lett. A.* **383**, 276–281 (2019) <https://doi.org/10.1016/j.physleta.2018.10.035>
27. Ellahi, R., Sait, S.M., Shehzad, N., Ayaz, Z.: A hybrid investigation on numerical and analytical solutions of electro-magnetohydrodynamics flow of nanofluid through porous media with entropy generation. *Int J Numer Meth Heat Fluid Flow.* **30**(2), 834–854 (2019) <https://doi.org/10.1108/HFF-06-2019-0506>
28. Majeed, A., Zeeshan, A., Bhatti, M.M., Ellahi, R.: Heat transfer in magnetite (Fe_3O_4) nanoparticles suspended in conventional fluids: refrigerant-134A ($\text{C}_2\text{H}_2\text{F}_4$), kerosene ($\text{C}_{10}\text{H}_{22}$), and water (H_2O) under the impact of dipole. *Heat Transf Res.* **51**(3), 217–232 (2020) <https://doi.org/10.1615/HeatTransRes.2019029919>
29. Sarafraz, M.M., Pourmehran, O., Yang, B., Arjomandi, M., Ellahi, R.: Pool boiling heat transfer characteristics of iron oxide nano-suspension under constant magnetic field. *Int. J. Therm. Sci.* **147**, 106131 (2020) <https://doi.org/10.1016/j.ijthermalsci.2019.106131>
30. Krishna, M.V., Chamkha, A.J.: Hall and ion slip effects on unsteady MHD convective rotating flow of nanofluids—application in biomedical engineering. *J Egyptian Math Soc.* **28**(1), 1 (2020) <https://doi.org/10.1186/s42787-019-0065-2>

Publisher's Note

Springer Nature remains neutral with regard to jurisdictional claims in published maps and institutional affiliations.